JGR Biogeosciences

RESEARCH ARTICLE
10.1029/2020JG005805

Processes Controlling Sea Surface pH and Aragonite Saturation State in a Large Northern Temperate Bay: Contrasting Temperature Effects

Liang Xue[1,2], Xufeng Yang[3], Yunxiao Li[4], Laoyu Li[1], Li-Qing Jiang[5,6], Ming Xin[1], Zongxing Wang[1], Xia Sun[1], and Qinsheng Wei[1]

[1]First Institute of Oceanography, Ministry of Natural Resources, Qingdao, China, [2]Laboratory for Regional Oceanography and Numerical Modeling, Qingdao National Laboratory for Marine Science and Technology, Qingdao, China, [3]Second Institute of Oceanography, Ministry of Natural Resources, Hangzhou, China, [4]Environment Science Laboratory, College of Resource and Environment, Shanxi Agricultural University, Taigu, China, [5]Earth System Science Interdisciplinary Center, University of Maryland, College Park, MD, USA, [6]National Centers for Environmental Information, National Oceanic and Atmospheric Administration, Silver Spring, MD, USA

Key Points:
- How the first and the second temperature effect would interact to influence seasonal variability of pH and Ω_{arag} is shown
- Contrast between the first temperature effects on pH and Ω_{arag} reduces seasonal amplitude of pH but increases seasonal amplitude of Ω_{arag}
- Processes controlling pH and Ω_{arag} variability from spring to summer in the JZB are quantified with a 1-D mass balance model

Supporting Information:
- Supporting Information S1
- Table S1

Correspondence to:
L. Xue and Q. Wei,
xueliang@fio.org.cn;weiqinsheng@fio.org.cn

Citation:
Xue, L., Yang, X., Li, Y., Li, L., Jiang, L.-Q., Xin, M., et al. (2020). Processes controlling sea surface pH and aragonite saturation state in a large northern temperate bay: Contrasting temperature effects. *Journal of Geophysical Research: Biogeosciences*, *125*, e2020JG005805. https://doi.org/10.1029/2020JG005805

Received 23 APR 2020
Accepted 28 MAY 2020
Accepted article online 8 JUN 2020

Abstract Understanding the natural variability of pH and aragonite saturation state (Ω_{arag}) is important for assessing ocean acidification (OA) impacts especially in the coastal ocean since anthropogenic CO_2 increase-induced OA is often superimposed by their natural variability. Here, we report the seasonal variability of sea surface pH and Ω_{arag} from spring to summer in the Jiaozhou Bay (JZB) and compare their controls based on two cruises conducted in April and August 2018. Results show that sea surface pH on the NBS scale slightly increases from 8.10 ± 0.05 in spring to 8.13 ± 0.04 in summer, whereas surface Ω_{arag} substantially increases from 2.05 ± 0.18 in spring to 3.34 ± 0.25 in summer. The difference in pH and Ω_{arag} seasonal increase is related to the contrasting temperature effects on them, which can be divided into the first temperature effect associated with acid-base equilibrium of the CO_2 system and the second temperature effect associated with CO_2 solubility-driven air-sea exchange. The two temperature effects have opposite influences on pH, canceling each other and causing a relatively small seasonal variability of pH, while they have consistent influences on Ω_{arag}, reinforcing each other and causing a relatively large variability of Ω_{arag}. Also, through both qualitative analyses and a 1-D model, we identify the processes controlling the seasonal variability of pH and Ω_{arag}. We find air-sea exchange dominates the seasonal variability of pH and Ω_{arag} in nearshore areas, while biological production is the most important in the central part of the JZB.

Plain Language Summary Both pH and saturation state of calcium carbonate ($CaCO_3$) minerals (Ω) are good metrics for ocean acidification (OA). Understanding their natural variability is important for assessing OA impacts especially on calcifying organisms in the coastal ocean since anthropogenic CO_2 increase-induced OA is often superimposed by their natural variability. Although a lot of work has been done, their controlling processes have not been well known. For example, how temperature would influence the seasonal variability of pH and Ω is poorly understood. Here, we divide temperature effects into two aspects: the first temperature effect associated with acid-base equilibrium of the CO_2 system and the second temperature effect associated with CO_2 solubility-driven air-sea exchange. We take the Jiaozhou Bay as an example to show that the two temperature effects have opposite influences on pH, canceling each other and causing a relatively small seasonal variability of pH, while the two temperature effects on aragonite saturation state (Ω_{arag}) reinforce each other, causing a relatively large variability of Ω_{arag}. Also, through both qualitative analyses and a 1-D model, we identify the processes controlling the seasonal variability of pH and Ω_{arag} including temperature variability, air-sea CO_2 exchange, terrestrial inputs, and biological processes. This study will improve the understanding of the natural variability of OA parameters and their controlling mechanisms.

1. Introduction

The ocean plays an important role in mitigating atmospheric carbon dioxide (CO_2) increase and has taken up ~30% of anthropogenic CO_2 since the beginning of the Industrial Revolution (Friedlingstein et al., 2019; Gruber et al., 2019). At the same time, the oceanic uptake of anthropogenic CO_2 changes its

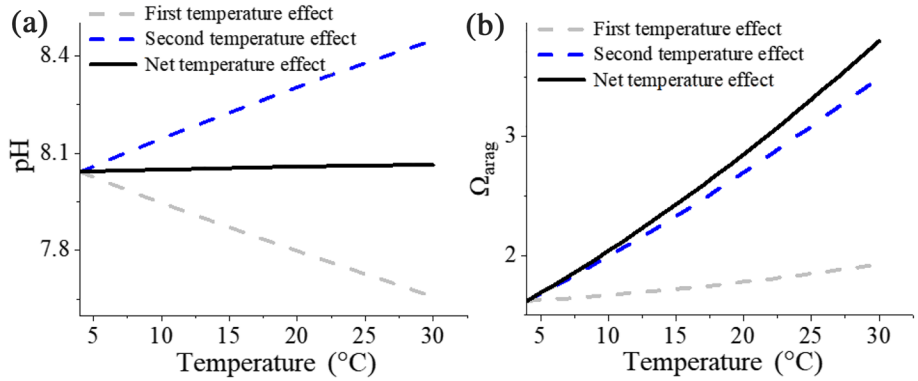

Figure 1. Schematics showing the temperature influence on (a) pH and (b) Ω_{arag}. The temperature influence includes the first temperature effect associated with acid-base equilibrium of the CO_2 system (gray line) and the second temperature effect associated with CO_2 solubility (blue line) as well as their net temperature effect (black line) (Jiang et al., 2019; Xue et al., 2017; Xue & Cai, 2020). Here constant TA (=2,300 μmol kg^{-1}), salinity (=35), DIC (=2,157.8 μmol kg^{-1} for the first temperature effect calculation), and pCO_2 (=395 μatm for the second temperature effect calculation) are used. Details can be found in section 2.3.

chemistry, causing increases in hydrogen ion concentrations ($[H^+]$) and thus decreases in pH, carbonate ion concentrations ($[CO_3^{2-}]$), and saturation state of calcium carbonate (Ω), a process called ocean acidification (OA) (Caldeira & Wickett, 2003; Doney et al., 2009). OA is usually characterized by decreases of pH or Ω over decades or longer time scales (Cooley et al., 2012). It may exert substantial influences on global ocean biogeochemical cycling and marine organisms as well as on ocean ecosystem services (Albright et al., 2018; Waldbusser et al., 2016).

Compared with the open ocean, it is more challenging to detect OA in coastal oceans due to the superimposition of natural variability of pH and Ω on the effect of anthropogenic CO_2 increase (e.g., Dong et al., 2017; Sutton et al., 2016). In the coastal ocean, seasonal temperature cycle, river inputs, upwelling, eutrophication, and biological production/respiration all can result in substantial natural variabilities of pH and Ω (Cai et al., 2011; Feely et al., 2008; Xu et al., 2017; Xue et al., 2017). Therefore, characterizing patterns of pH and Ω variability is of great importance for assessing OA impacts especially on calcifying organisms and for improving experiment design designated to study organisms' response to OA (Fassbender et al., 2016; Sutton et al., 2016).

Although a lot of work has been done to understand the natural variability of pH and Ω (e.g., Hagens & Middelburg, 2016; Jiang et al., 2019; Omar et al., 2016; Xue et al., 2018), their controlling processes have not been well known. For example, both pH and Ω are good metrics for OA because they respond similarly to the addition/removal of CO_2, but how temperature would influence their seasonal variability is poorly understood. In the respect of temperature-driven acid-base equilibrium of CO_2 system ($CO_2 + H_2O \rightleftharpoons H_2CO_3 \rightleftharpoons H^+ + HCO_3^- \rightleftharpoons CO_3^{2-} + 2H^+$), which can be called the first temperature effect or "internal temperature effect," increasing temperature would increase $[H^+]$ and $[CO_3^{2-}]$, thus decreasing pH but increasing Ω (Figure 1). In the respect of CO_2 solubility-driven air-sea CO_2 exchange, which can be called the second temperature effect or "external temperature effect," increasing temperature allows a body of water to release more CO_2 in order to maintain equilibrium with the atmosphere, thus decreasing seawater CO_2 concentration and increasing both pH and Ω (Figure 1). The contrasting influence of the first temperature effects on pH and Ω may cause differences of temperature roles in the seasonal variability of pH and Ω. However, how the first and the second temperature effects would interact to influence them is unknown. Note the temperature effects in this work only refer to chemical equilibrium and air-sea exchange directly associated with temperature (Jiang et al., 2019; Xue et al., 2017; Xue & Cai, 2020) and do not include other indirect temperature effects such as influences on the growth of marine phytoplankton.

The Jiaozhou Bay (JZB, 35°57′ to 36°18′N, 120°04′ to 120°23′E), located on the western coast of the Yellow Sea, China (Figure 2), is a shallow semienclosed water body with an average water depth of ~7 m. The JZB is dominated by the East Asian monsoon, with a southerly or southeasterly wind in

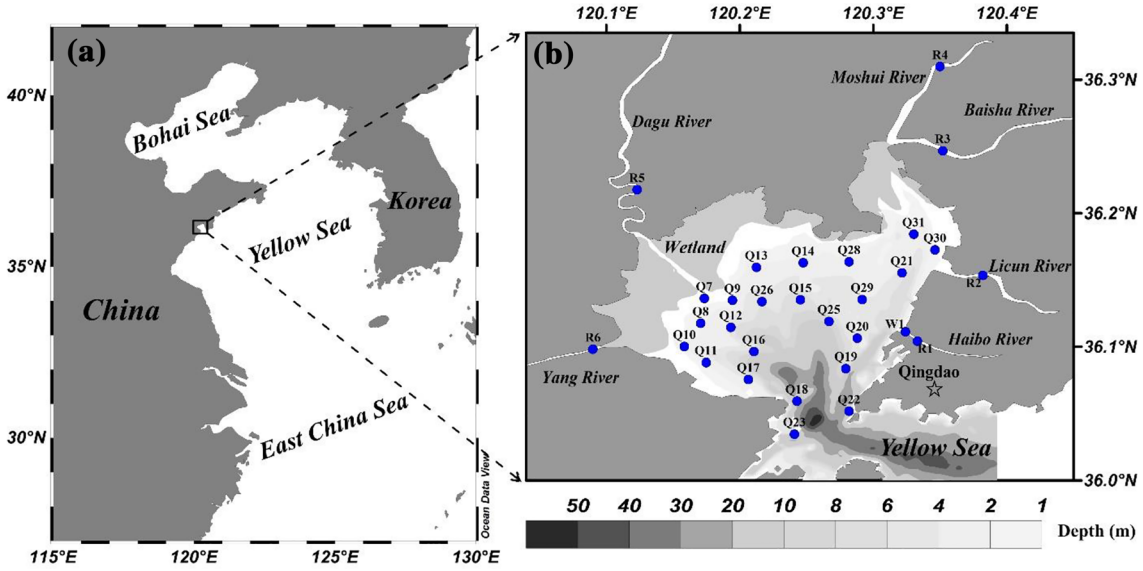

Figure 2. Study site. Panel (a) shows the relative location of the study site (within the black frame) in the eastern part of China coastal oceans, and panel (b) shows the study site and sampling stations (blue dots) in the JZB and adjacent estuaries. Also, water depths of the JZB are shown with color bar in panel (b).

spring and summer and a northerly or northwesterly wind in fall and winter. The JZB is featured by a semidiurnal tide with an average tidal range of 2.7–3.0 m and a maximum of 5.1 m (Zhang, 2007). The tide results in strong turbulent mixing and nearly homogeneous vertical profiles of temperature and salinity. Even in summer when the freshwater discharge to the bay reaches its maximum, the stratification is very weak (Chen et al., 1999).

The JZB is an ideal site for characterizing the natural variability of pH and Ω and understanding their controlling processes, particularly the interaction between the first and the second temperature effects. First, the JZB as a midlatitude water body has a strong seasonal signal both physically and biogeochemically. For example, on average from spring to summer, sea surface temperature (SST) would increase by ~15°C (Deng et al., 2016), and primary production would increase from 406.0 mg C m^{-2} d^{-1} in spring to 630.2 mg C m^{-2} d^{-1} in summer (Fu et al., 2009). Second, the JZB is seriously disturbed by human activities such as the overloading of nutrients and carbon (Li et al., 2018; Yang et al., 2018).

The JZB is surrounded by Qingdao, a city with rapid economic development and population growth in North China, and just to the south is connected with the Yellow Sea via a narrow channel of ~2.5 km (Figure 2). There are more than 10 seasonal rivers flowing into the JZB, including the Dagu River, the Licun River, and the Haibo River (Figure 2), but these rivers have no natural runoff during most of the time of a year. Instead, most of the middle and lower reaches of these rivers have become conduits for wastewater and sewage, through which about 75% of the urban sewage flows into the JZB every year (Gao et al., 2008). Furthermore, the JZB is also an important shellfish-farming area (Yang et al., 2007), where scallop and clam, etc., are vulnerable to low pH and Ω. During the past decades, the JZB has received special attention in terms of CO_2 dynamics (e.g., Deng et al., 2016; Li et al., 2007, 2017; Yang et al., 2018), yet there is a poor understanding of the seasonal variability of pH and Ω and especially their controlling processes.

In this study, we report the seasonal variability of sea surface pH and Ω from spring to summer in the JZB and identify their controls based on two cruises conducted in April and August 2018, respectively (Figure 2). Our main focus is to compare the controlling processes of surface pH and Ω via both qualitative analyses and a 1-D model and especially to clarify how the first and the second temperature effects would interact to influence the seasonal variability of pH and Ω. This work would improve the understanding of the natural variability of acidification parameters and their controlling mechanisms.

2. Materials and Methods

2.1. Sample Collection and Measurement

We conducted two cruises aboard a fishing vessel during 25–26 April and 3–4 August 2018, respectively. During the two cruises, the locations of sampling stations are completely the same, and, in each cruise, there are 23 sampling stations (Figure 2). At each station, just surface samples are collected for dissolved oxygen (DO), pH, and total dissolved inorganic carbon (DIC) using a Van Dorn water sampler since water column is vertically well mixed (Chen et al., 1999). Also, during 26–27 July 2018, we collected water samples for DO, pH, and DIC measurements in the six main estuaries around the JZB (Figure 2).

SST and sea surface salinity (SSS) are measured using YSI 6600, with a nominal precision of 0.01°C and 0.01 psu, respectively. DO is measured with the classic Winkler method as described by Wei et al. (2019). Also, apparent oxygen utilization (AOU) is calculated by subtracting measured DO content from saturated oxygen in seawater at a given potential temperature and salinity (Benson & Krause, 1984). pH on the NBS (NIST) scale is measured at a constant temperature of 25°C ($pH_{@25}$) using an Orion 3-Star plus pH Benchtop meter with a ROSS pH combination electrode (Thermo Fisher Scientific, USA). pH electrode is calibrated and checked before and after measurements using the pH buffer solutions with pH values of 4.01, 7.00, and 10.01 at 25°C (Thermo Fisher Scientific, USA). The pH measurement is repeated at least three times for each sample with a precision and accuracy of ±0.01 (Zhao et al., 2020). Samples for DIC measurement are stored in 20-ml vials at 4°C until laboratory analysis after poisoned by 10 μl saturated mercuric chloride solution. DIC is measured within 1 week with a DIC analyzer (AS-C3, Apollo SciTech, USA) by acidifying 0.5–0.8 ml of water samples and quantifying the released CO_2. The DIC measurement is repeated at least three times for each sample with a precision of better than 0.1% and an overall accuracy of ~2 μmol kg^{-1} (Cai et al., 1998). Throughout the DIC analysis, certified reference materials (CRMs, Batch 173) from Scripps Institution of Oceanography are used to serve as the standard solutions.

2.2. Calculation of Aragonite Saturation State (Ω_{arag}) and Other Carbonate Parameters

Considering that aragonite and calcite are two common polymorphs of calcium carbonate ($CaCO_3$) in the ocean (Morse et al., 2007) and aragonite is more soluble than calcite (Mucci, 1983), in this work, we just discuss Ω_{arag}. Ω_{arag} is defined by

$$\Omega_{arag} = \left[CO_3^{2-}\right] \times \left[Ca^{2+}\right] / K^*_{sp}, \quad (1)$$

where $[Ca^{2+}]$ is the calcium concentration and K^*_{sp} is the apparent solubility product of aragonite (Mucci, 1983).

$[Ca^{2+}]$ is calculated from salinity using the ratio between $[Ca^{2+}]$ and salinity in the JZB (311.94 × salinity μmol kg^{-1}) (Zhang et al., 1992), and K^*_{sp} is calculated after Mucci (1983). $[CO_3^{2-}]$ is calculated from temperature, salinity, $pH_{@25}$, and DIC using the CO2SYS program (Lewis et al., 1998) with the apparent dissociation constants (K^*_1 and K^*_2) for carbonic acid of Mehrbach et al. (1973) as refitted by Dickson and Millero (1987) and the CO_2 solubility constant (K_0) of Weiss (1974). Meanwhile, we calculate Ω_{arag} at in situ temperature ($\Omega_{arag@in\ situ}$) and at a constant temperature of 25°C ($\Omega_{arag@25}$), pH at in situ temperature ($pH_{@in\ situ}$), surface partial pressure of CO_2 (pCO_2), and total alkalinity (TA), parts of which are shown in Figure S1 in the supporting information.

2.3. Estimation of Temperature Effects on Seasonal Variability of pH and Ω_{arag}

Temperature can influence the composition and concentration of CO_2 species, thus altering pH and Ω_{arag} by (I) acid-base equilibrium of the CO_2 system under conditions of constant TA and DIC and by (II) CO_2 solubility-driven air-sea exchange that just changes DIC but not TA (Jiang et al., 2019; Xue et al., 2017; Xue & Cai, 2020). To clearly show how temperature will influence pH and Ω_{arag}, in this work, we artificially divide the temperature effect into two types, which factually coexist in the ocean. The first temperature effect just changes internal allocation of CO_2 system species (i.e., bicarbonate ion (HCO_3^-), CO_3^{2-}, and CO_2) under conditions of constant TA and DIC, like a parcel of water in a closed system, and is termed the "internal temperature effect." The second temperature effect would influence CO_2 release to the atmosphere or CO_2 uptake by the ocean by changing CO_2 solubility and is realized via air-sea exchange, like a parcel of water in an open system, which is termed the "external temperature effect." In addition, both pH and

Ω_{arag} can be expressed as a function of DIC and TA at given salinities (S) and temperatures (T) (e.g., Xue et al., 2016a), that is, f(DIC, TA, S, T), when [Ca^{2+}] is conservative with respect to salinity, and can be calculated using the CO2SYS program (Lewis et al., 1998). Here we take pH as an example and show how to estimate the two temperature effects on the seasonal variability of pH (similar calculation is done for Ω_{arag}). We set the springtime as time t_1, at which T, S, and carbonate parameters (TA, DIC, pH, Ω_{arag}) are T_1, S_1, TA_1, DIC_1, pH_1, and $(\Omega_{arag})_1$, respectively, and the summertime as time t_2, at which these parameters change to T_2, S_2, TA_2, DIC_2, pH_2, and $(\Omega_{arag})_2$ (also hereafter).

a. First temperature effect: To determine the first temperature effect on the seasonal variability of pH (ΔpH_{tem1}), we calculate pH at temperature T_2 by keeping DIC, TA, and S constant and just allowing temperature to change ($f(DIC_1, TA_1, S_1, T_2)$). Thus, the first temperature effect on pH variability can be calculated using Equation 2a:

$$\Delta pH_{tem1} = f\ (DIC_1, TA_1, S_1, T_2) - pH_1 \tag{2a}$$

b. Second temperature effect: To give a first-order estimate of the second temperature effect on the seasonal variability of pH (ΔpH_{tem2}), according to Xue et al. (2017) and Jiang et al. (2019), we calculate pH by keeping pCO_2, TA, and S constant and allowing DIC to change with temperate on the assumption there is a transient air-sea CO_2 equilibrium under conditions of different temperatures. Specifically, we first calculate DIC values (DIC_e) at temperatures T_1 and T_2 from constant pCO_2, TA, and S (Equations 2b and 2c) and then calculate pH at temperature T_1 from constant TA and changing DIC_e (Equation 2d) using the CO2SYS program (Lewis et al., 1998). Thus, the second temperature effect on pH variability can be estimated using Equation 2d. Accordingly, the net temperature effect on pH (ΔpH_{tem}), that is, the total effect of the two temperature effects, can be estimated using Equation 2e.

$$DIC_{e1} = fuc\ (pCO_2, TA_1, S_1, T_1), \tag{2b}$$

$$DIC_{e2} = fuc\ (pCO_2, TA_1, S_1, T_2), \tag{2c}$$

$$\Delta pH_{tem2} = f\ (DIC_{e2}, TA_1, S_1, T_1) - f\ (DIC_{e1}, TA_1, S_1, T_1), \tag{2d}$$

$$\Delta pH_{tem} = f\ (DIC_{e2}, TA_1, S_1, T_2) - f\ (DIC_{e1}, TA_1, S_1, T_1), \tag{2e}$$

where fuc (pCO_2, TA, S, T) is DIC as a function of pCO_2, TA, S, and T; DIC_{e1} and DIC_{e2} are DIC values at temperatures T_1 and T_2 calculated from constant pCO_2, TA, and S.

In this work, mean atmospheric CO_2 concentration (420 parts per million, i.e., ppm) during the April cruise in the JZB measured using an infrared CO_2 detector (Li-Cor 7000) is used as the constant pCO_2. Note that in real ocean, it is almost impossible to reach transient air-sea CO_2 equilibrium due to the slow air-sea CO_2 exchange (Sarmiento & Gruber, 2006), which will lead to overestimation or underestimation of DIC_e. However, this influence on ΔpH_{tem2} is minor since this overestimated or underestimated part would be to a large extent canceled each other as shown from Equation 2d. This is verified by the insensitivity of ΔpH_{tem2} to pCO_2 variability, for example, from 300 to 500 μatm (Table S1). Thus, this method is feasible for providing a first-order estimate of the second temperature effect on pH variability.

2.4. A 1-D Mass Budget Model for Quantifying Processes Influencing Seasonal Variability of pH and Ω_{arag}

Following Xue et al. (2016b) and Xue et al. (2017), we use a 1-D mass budget model to estimate the contributions from temperature, air-sea exchange, mixing between terrestrial inputs and ocean, biological production/respiration, and calcium carbonate ($CaCO_3$) formation/dissolution to seasonal variability of pH and Ω_{arag} in the JZB. Here, we take pH as an example and show how to quantify the processes influencing the seasonal variability of pH (similar calculation is done for Ω_{arag}).

Seasonal variability of DIC, TA, pH, and Ω_{arag} can be expressed as follows:

$$\Delta DIC = DIC_2 - DIC_1 = \Delta DIC_{a-s} + \Delta DIC_{mix} + \Delta DIC_{bio} + \Delta DIC_{cal}, \quad (3a)$$

$$\Delta TA = TA_2 - TA_1 = \Delta TA_{mix} + \Delta TA_{bio} + \Delta TA_{cal}, \quad (3b)$$

$$\Delta pH = pH_2 - pH_1 = \Delta pH_{tem} + \Delta pH_{a-s} + \Delta pH_{mix} + \Delta pH_{bio} + \Delta pH_{cal} + \Delta pH_{non}, \quad (3c)$$

$$\Delta\Omega_{arag} = (\Omega_{arag})_2 - (\Omega_{arag})_1 = \Delta\Omega_{tem} + \Delta\Omega_{a-s} + \Delta\Omega_{mix} + \Delta\Omega_{bio} + \Delta\Omega_{cal} + \Delta\Omega_{non}, \quad (3d)$$

where subscripts "tem," "a-s," "mix," "bio," and "cal" denote temperature variability, air-sea exchange, mixing, biological production/respiration, and $CaCO_3$ formation/dissolution, respectively, and the sign "Δ" denotes the net change of a parameter from spring to summer. ΔpH_{non} (or $\Delta\Omega_{non}$) is a nonlinear interaction term, the difference between ΔpH (or $\Delta\Omega_{non}$) and the sum of pH (or Ω) change due to each process, considering that pH and Ω_{arag} are not linear.

In the following, we briefly show how to estimate the contribution of each process to pH variability from spring to summer.

a. Temperature: Since the second temperature effect is closely related to air-sea exchange, in the 1-D model, the second temperature effect is attributed to air-sea exchange term, and temperature effect only refers to the first temperature effect. That is, in the 1-D model, the temperature effect is quantified by Equation 2a. Additionally, since the temperature effect has been quantified here, subsequently the four processes (air-sea exchange, mixing, biological production/respiration, and $CaCO_3$ formation/dissolution) are dealt with under isothermal conditions.
b. Air-sea exchange: Air-sea CO_2 exchange changes DIC, but not TA.

$$\Delta DIC_{a-s} = -F \times (t_2 - t_1)/(D \times H), \quad (4a)$$

$$(DIC_2)_{a-s} = DIC_1 + \Delta DIC_{a-s}, \quad (4b)$$

$$\Delta pH_{a-s} = f\left((DIC_2)_{a-s}, TA_1, S_1, T_1\right) - pH_1, \quad (4c)$$

where F is the air-sea CO_2 flux calculated based on air-sea pCO_2 gradient and the gas transfer velocity formula of Sweeney et al. (2007). Mean atmospheric CO_2 concentrations in the JZB during the cruises of April and August 2018 were 420 and 408 ppm, respectively, which are measured using an infrared CO_2 detector (Li-Cor 7000), and corresponding sea surface pCO_2 is calculated from pH and DIC (Figure S1). Climatological mean wind speeds during April (6.0 m s^{-1}) and August (4.6 m s^{-1}) in the JZB are used. D is the seawater density, and H is the mixed layer depth, which is the water depth in the well-mixed JZB; $(DIC_2)_{a\text{-}s}$ is the predicted DIC at time t_2 due solely to air-sea exchange from time t_1 to t_2

c. Mixing: we attribute salinity changes solely to mixing between terrestrial inputs and ocean (horizontal mixing), neglecting the other processes including evaporation and precipitation. Thus, DIC and TA changes due to mixing can be estimated as follows:

$$\Delta DIC_{mix} = (DIC_{oce} - DIC_{ter})/(S_{oce} - S_{ter}) \times (S_2 - S_1), \quad (5a)$$

$$\Delta TA_{mix} = (TA_{oce} - TA_{ter})/(S_{oce} - S_{ter}) \times (S_2 - S_1), \quad (5b)$$

$$DIC_{2mix} = DIC_1 + \Delta DIC_{mix}, \quad (5c)$$

$$(TA_2)_{mix} = TA_1 + \Delta TA_{mix}, \quad (5d)$$

$$\Delta pH_{mix} = f\left((DIC_2)_{mix}, (TA_2)_{mix}, S_2, T_1\right) - pH_1, \quad (5e)$$

where DIC_{oce} and DIC_{ter} are DIC at the ocean and terrestrial end-members, respectively; TA_{oce} and TA_{ter} are TA at the ocean and terrestrial end-members, respectively; S_{oce} and S_{ter} are salinity at the ocean and terrestrial end-members, respectively. $(DIC_2)_{mix}$ is the predicted DIC at time t_2 due only to mixing from time t_1 to t_2, and similarly, $(TA_2)_{mix}$ is the predicted TA at time t_2.

During summertime, we select stations at the Bay mouth (Station G22) and estuaries surrounding the JZB as the ocean and terrestrial end-members, respectively, where S_{oce} = 31.55, TA_{oce} = 2,358 μmol kg^{-1},

Table 1
Surface Temperature (Temp, °C), Salinity (Sal, psu), In Situ Temperature pH on the NBS Scale ($pH_{@in\ situ}$), Total Dissolved Inorganic Carbon (DIC, μmol kg^{-1}), and Total Alkalinity (TA, μmol kg^{-1}) in the Six Main Estuaries Around the JZB and in a Sewage Outlet Within the Haibo River (W1) During 26–27 July 2018

Station	Temp	Sal	$pH_{@in\ situ}$	DIC	TA
W1 (sewage outlet)	29.3	1.30	6.93	4,179	3,369
R1 (Haibo River)	32.5	20.80	7.10	3,312	3,111
R2 (Licun River)	29.3	0.40	7.41	3,631	3,330
R3 (Baisha River)	30.4	0.39	7.57	2,821	2,665
R4 (Moshui River)	31.6	0.68	8.89	2,657	2,833
R5 (Dagu River)	29.6	16.51	7.79	2,874	2,934
R6 (Yang River)	30.8	13.14	7.92	2,772	2,858

Note. Locations are shown in Figure 1.

$DIC_{oce} = 2{,}101\ \mu mol\ kg^{-1}$, $S_{ter} = 0.69 \pm 0.43$, $TA_{ter} = 3{,}049 \pm 354\ \mu mol\ kg^{-1}$, and $DIC_{ter} = 3{,}322 \pm 712\ \mu mol\ kg^{-1}$. The average of salinity, TA, and DIC in a sewage outlet within the Haibo River (Station W1) and three estuaries with low salinities of <2 (Licun River, Baisha River, and Moshui River) along the eastern coast (Figure 2 and Table 1) is used as the average terrestrial end-member values (Table 1).

d. $CaCO_3$ formation/dissolution:

Since the TA change due to biological production/respiration is relatively minor ($\Delta TA_{bio} = -17/106 * \Delta DIC_{bio}$) if the Redfield ratio is assumed (Redfield et al., 1963), here we ignore this biological effect on TA (Xue et al., 2016b). Thus, Equation 3b can be written as

$$\Delta TA_{cal} = \Delta TA - \Delta TA_{mix}. \tag{6a}$$

Given that during $CaCO_3$ formation/dissolution TA and DIC would change with a ratio of 2:1 (Chen, 1978), thus we can obtain

$$\Delta DIC_{cal} = 0.5{*}\Delta TA_{cal}, \tag{6b}$$

$$(TA_2)_{cal} = TA_1 + \Delta TA_{cal}, \tag{6c}$$

$$(DIC_2)_{cal} = DIC_1 + \Delta DIC_{cal}, \tag{6d}$$

$$\Delta pH_{cal} = f\left((DIC_2)_{cal}, (TA_2)_{cal}, S_1, T_1\right) - pH_1, \tag{6e}$$

where $(DIC_2)_{cal}$ is the predicted DIC at time t_2 due only to $CaCO_3$ formation/dissolution from time t_1 to t_2, and similarly, $(TA_2)_{cal}$ is the predicted TA at time t_2.

e. Biological production/respiration: We assign the rest of DIC change to biological production/respiration to close the budget.

Thus,

$$\Delta DIC_{bio} = \Delta DIC - (\Delta DIC_{a-s} + \Delta DIC_{mix} + \Delta DIC_{cal}), \tag{7a}$$

$$(DIC_2)_{bio} = DIC_1 + \Delta DIC_{bio}, \tag{7b}$$

$$\Delta pH_{bio} = f\left((DIC_2)_{bio}, TA_1, S_1, T_1\right) - pH_1, \tag{7c}$$

where $(DIC_2)_{bio}$ is the predicted DIC at time t_2 only due to biological production/respiration from time t_1 to t_2.

Also, relative importance of temperature variability ($\%\Delta pH_{tem}$ and $\%\Delta\Omega_{tem}$), air-sea exchange ($\%\Delta pH_{a-s}$ and $\%\Delta\Omega_{a\text{-}s}$), mixing ($\%\Delta pH_{mix}$ and $\%\Delta\Omega_{mix}$), biological production/respiration ($\%\Delta pH_{bio}$ and $\%\Delta\Omega_{bio}$), and calcium carbonate formation/dissolution ($\%\Delta pH_{cal}$ and $\%\Delta\Omega_{cal}$) to pH and Ω_{arag} variability from spring to summer as well as the nonlinear term ($\%\Delta pH_{non}$ and $\%\Delta\Omega_{non}$) is calculated as

$$100 \times X_i / \sum_{i=1}^{6} |X_i|. \tag{8}$$

where X_i is pH or Ω_{arag} change due to one process (the nonlinear term included).

3. Results and Discussion

3.1. Distributions of SST, SSS, and AOU

SST substantially increases from an average of 12.43 ± 0.89°C in spring to an average of 27.34 ± 0.35°C in summer (Figure 3 and Table 2). Spatially, during spring, SST is high adjacent to land and is low in the central part of the study area (Figure 3a). During summer, SST distribution is relatively homogeneous (Figure 3b).

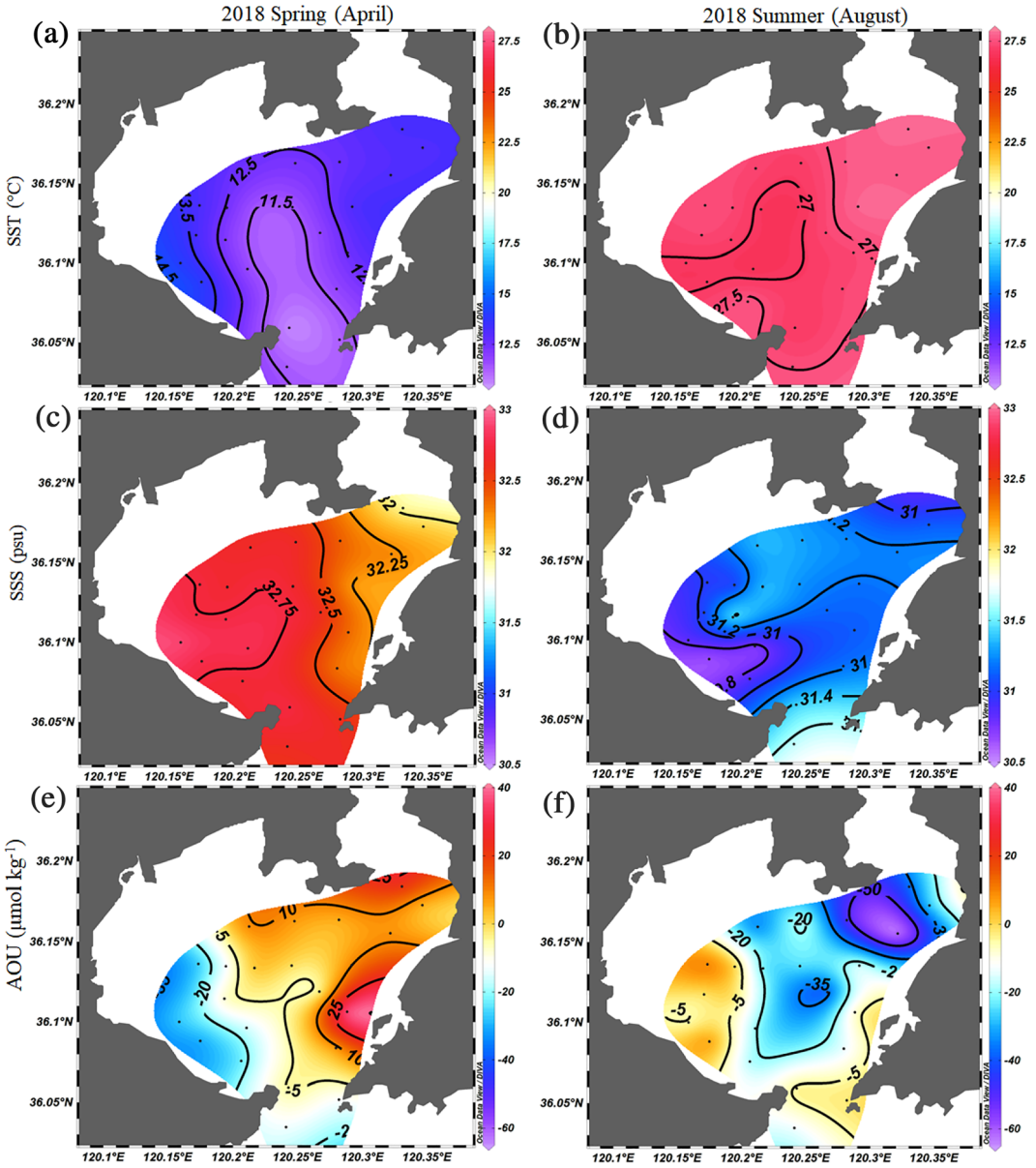

Figure 3. Spatial distributions of (a,b) SST, (c,d) SSS, and (e,f) AOU during spring and summer 2018 in the JZB.

In contrast, SSS obviously decreases from an average of 32.57 ± 0.25 psu in spring to an average of 31.16 ± 0.25 psu in summer (Figure 3 and Table 2). Spatially, during spring, SSS is high in the western part of the study area and is low in the eastern and northeastern part (Figure 3c) due to influences of sewage discharge from wastewater treatment plants surrounding the JZB (Yang et al., 2018). During summer, very low SSS is observed in the west (Figure 3d) possibly due to influence of land runoff.

From spring to summer, AOU becomes more negative with an average of −3.76 ± 17.04 μmol kg^{-1} in spring and an average of −17.17 ± 18.38 μmol kg^{-1} in summer (Figure 3 and Table 2), indicating that there may be a net biological production from spring to summer. Spatially, during spring, AOU shows negative values in the west and positive values in the north and east (Figure 3e). During summer, AOU is negative in the whole study area with more negative values in the north and northeast (Figure 3f).

3.2. Distributions of Sea Surface DIC, pH, and Ω_{arag}

Sea surface DIC decreases from an average of 2,183 ± 23 μmol kg^{-1} in spring to an average of 2,054 ± 38 μmol kg^{-1} in summer (Figure 4 and Table 2). Generally, the spatial distribution of DIC is

Table 2
Average of Sea Surface Temperature (SST), Salinity (SSS), Apparent Oxygen Utilization (AOU), Surface Partial Pressure of CO_2 (pCO_2), Total Alkalinity (TA), Total Dissolved Inorganic Carbon (DIC), pH at 25°C on the NBS Scale ($pH_{@25}$), pH at In Situ Temperature ($pH_{@in\ situ}$), Seawater Saturation State With Respect to the Mineral Aragonite at 25°C ($\Omega_{arag@25}$) and at In Situ Temperature ($\Omega_{arag@in\ situ}$) During Spring (April) and Summer (August) 2018 in the JZB

	Spring	Summer	Difference
SST (°C)	12.43 ± 0.89	27.34 ± 0.35	14.91 ± 0.86
SSS (psu)	32.57 ± 0.25	31.16 ± 0.25	−1.41 ± 0.37
AOU (μmol kg^{-1})	−3.76 ± 17.04	−17.17 ± 18.38	−13.41 ± 30.64
pCO_2 (μmol kg^{-1})	493 ± 72	494 ± 50	1 ± 88
TA (μmol kg^{-1})	2,346 ± 19	2,311 ± 36	−34 ± 38
DIC (μmol kg^{-1})	2,183 ± 23	2054 ± 38	−130 ± 41
$pH_{@25}$	7.94 ± 0.04	8.16 ± 0.04	0.22 ± 0.06
$pH_{@in\ situ}$	8.10 ± 0.05	8.13 ± 0.04	0.03 ± 0.07
$\Omega_{arag@25}$	2.23 ± 0.19	3.28 ± 0.24	1.05 ± 0.34
$\Omega_{arag@in\ situ}$	2.05 ± 0.18	3.34 ± 0.25	1.29 ± 0.34

Note. The seasonal variability from spring to summer is also shown (Difference).

relatively homogeneous. During spring, surface DIC is high in the northeastern part of the study area with DIC values of 2,190–2,240 μmol kg^{-1} and is low in other parts with DIC values of 2,140–2,165 μmol kg^{-1} (Figure 4a). During summer, low DIC values of <2,040 μmol kg^{-1} are observed in the north (Figure 4b).

From spring to summer, sea surface $pH_{@25}$ shows a large increase, with an average of 7.94 ± 0.04 in spring and an average of 8.16 ± 0.04 in summer (Figure 4 and Table 2). Spatially, during spring, surface $pH_{@25}$ is slightly high in the central part of the study area and low in the west and in the northeast (Figure 4c). During summer, surface $pH_{@25}$ is slightly high in the north and low in the northeast (Figure 4d). Compared to $pH_{@25}$, from spring to summer, sea surface $pH_{@in\ situ}$ just shows a small increase, with an average of 8.10 ± 0.05 in spring and an average of 8.13 ± 0.04 in summer (Figure 4 and Table 2). The spatial pattern of $pH_{@in\ situ}$ is similar to that of $pH_{@25}$ (Figures 4c–4f).

In contrast to pH, both $\Omega_{arag@25}$ and $\Omega_{arag@in\ situ}$ show a substantial seasonal increase ($\Omega_{arag@25}$ distribution is very similar to $\Omega_{arag@in\ situ}$ and thus just shown in Figure S1). Surface $\Omega_{arag@25}$ increases from 2.23 ± 0.19 in spring to 3.28 ± 0.24 in summer, and surface $\Omega_{arag@in\ situ}$ increases from 2.05 ± 0.18 in spring to 3.34 ± 0.25 in summer (Figure 4 and Table 2). The spatial patterns of both $\Omega_{arag@25}$ and $\Omega_{arag@in\ situ}$ are similar to those of $pH_{@25}$ (Figure 4 and Figure S1). During spring, surface $\Omega_{arag@25}$ and $\Omega_{arag@in\ situ}$ are high in the central part of the study area and low in the west and in the northeast. During summer, surface $\Omega_{arag@25}$ and $\Omega_{arag@in\ situ}$ are high in the north and low in the northeast and the southwest. Overall, surface DIC, pH, and Ω_{arag} from spring to summer exhibit an obvious seasonal variability, and their spatial distributions are relatively homogeneous. Thus, hereafter, we focus on the processes that control the seasonal variability of pH and Ω_{arag}.

3.3. Influences of Temperature and Air-Sea Exchange on Seasonal Variability of pH and Ω_{arag}

3.3.1. Interaction Between the First and the Second Temperature Effects

To qualitatively analyze the temperature influence on pH and Ω_{arag}, with the method described in section 2.3 (Equations 2b–2e), we use the mean value during the cruise of April 2018 as the starting point of calculation and simulate pH and Ω_{arag} variability solely due to the first, the second, and the net temperature effects (Figures 5a–5d). We find that the simulated $pH_{@in\ situ}$ and $\Omega_{arag@in\ situ}$ due only to net temperature effect and the simulated $pH_{@25}$ and $\Omega_{arag@25}$ due only to the second temperature effect are generally in agreement with their respective observational mean values in August 2018. It demonstrates that SST variability may play a dominant role in the seasonal variability of pH and Ω_{arag} from April to August in the JZB.

However, factually, temperatures exert different influences on the seasonal variability of pH and Ω_{arag}. An obvious difference is that the first temperature effect has opposite influences on pH and Ω_{arag}, which would cause differences in their net temperature effect and even influence their amplitude of seasonal variability (Figure 5). Specifically, the first and the second temperature effects have opposite influences on pH, which would cancel out each other and result in a relatively small net effect. Using the method described in section 2.3, we find that in the JZB when SST on average increases by ~15°C from April to August (Table 2), the first temperature effect would decrease pH by 0.19 ± 0.01 but the second temperature effect would increase pH by 0.23 ± 0.01 (Figure 5 and Table 3). As a result, most part of the second temperature effect on pH is canceled out by the first temperature effect, which makes the net temperature effect just induce a pH increase of ~0.04 (0.23–0.19 = 0.04). In contrast, the first and the second temperature effects have consistent influences on Ω_{arag}, which would reinforce each other and result in a relatively large net effect. When SST increases by ~15°C from April to August (Table 2), the first and the second temperature effects would increase Ω_{arag} by 0.23 ± 0.02 and 1.22 ± 0.07, respectively (Figure 5 and Table 3). Due to the aggravation between the first and the second temperature effect on Ω_{arag}, the net temperature effect would make Ω_{arag} increase by ~1.45 (0.23 + 1.22 = 1.45). Clearly, no matter pH or Ω_{arag}, in the JZB from spring to summer, the second temperature effect is larger than the first temperature effect in absolute values (Figure 5

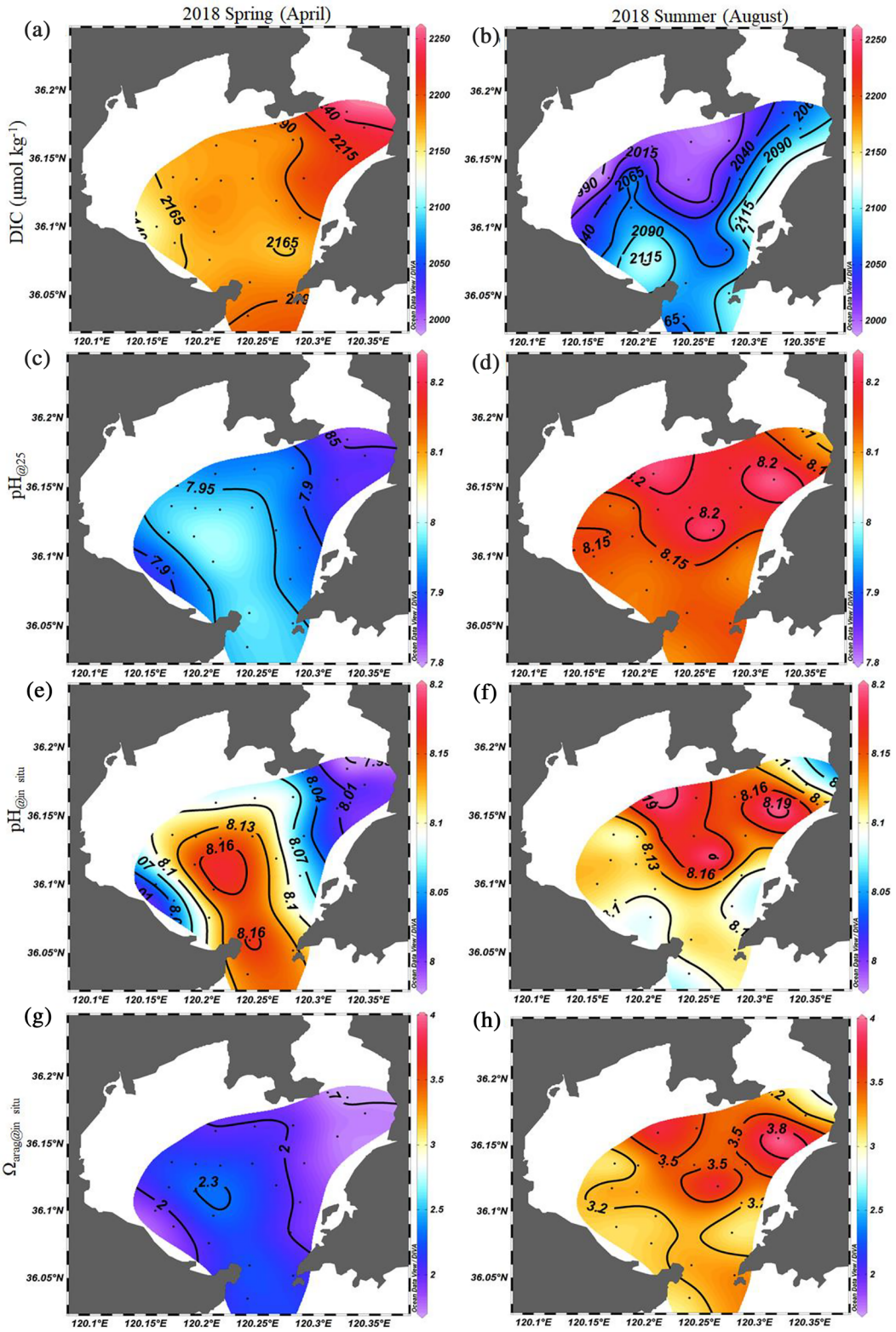

Figure 4. Spatial distributions of (a,b) sea surface DIC, (c,d) $pH_{@25}$, (e,f) $pH_{@in\ situ}$, and (g,h) $\Omega_{arag@in\ situ}$ during spring and summer 2018 in the JZB.

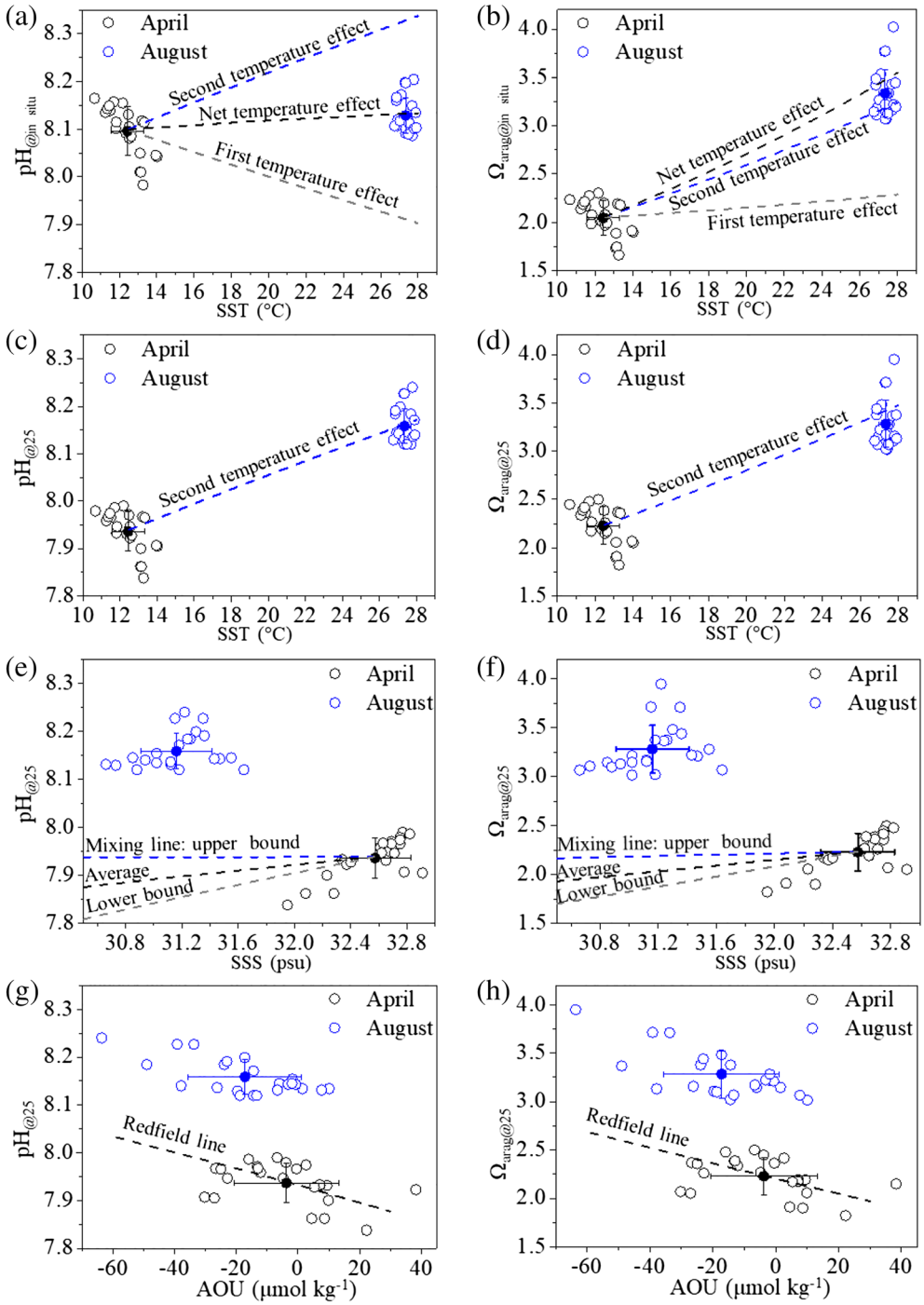

Figure 5. Property-property plots of $pH_{@in\ situ}$, $pH_{@25}$, $\Omega_{arag@in\ situ}$, and $\Omega_{arag@25}$ with (a–d) SST, (e,f) SSS, and (g,h) AOU for the data collected during April (black empty circle) and August (blue empty circle) 2018 in the JZB. Solid circles in each panel denote mean values of related parameters during the April and August cruises. Dashed lines denote simulated pH and Ω_{arag} variability solely due to the first temperature effect, second temperature effect, net temperature effect (a–d), theoretical mixing between terrestrial inputs and ocean (mixing line) (e,f), and biological production/respiration (Redfield line) (g,h). These dashed lines start from the mean value during April cruise (the starting point of calculation), and more details can be found in sections 2.3 and 2.4. In panels (e) and (f), we use the mean of salinity (0.69 ± 0.43), TA (3,049 ± 354 μmol kg^{-1}), and DIC (3,322 ± 712 μmol kg^{-1}) in a sewage outlet within the Haibo River (station W1) and three estuaries with low salinities of <2 (Licun River, Baisha River, and Moshui River) as the average terrestrial end-member values (Table 1) and use the average plus standard deviation and average minus standard deviation as the upper and lower bounds of terrestrial end-member values, respectively. Thus, the black dashed line denotes average mixing, and the blue and gray dashed lines denote the upper and lower bounds of mixing, respectively. In panels (g) and (h), change in pH and Ω_{arag} due only to biological production/respiration indicated by AOU is calculated based on the classic Redfield ratio of DIC: AOU = 106:138.

Table 3
Regionally Averaged Contribution of Temperature Variability, Air-Sea Exchange, Mixing Between Terrestrial Inputs and Ocean, Biological Production/Respiration, and Calcium Carbonate ($CaCO_3$) Formation/Dissolution to pH and Ω_{arag} Variability From Spring to Summer (ΔpH and $\Delta\Omega$) as well as the Nonlinear Term

	ΔpH	%ΔpH	ΔΩ	%ΔΩ
[a] (first) Temperature effect (tem)	−0.19 ± 0.01	−28.29 ± 5.91	0.23 ± 0.02	9.34 ± 2.18
Second temperature effect	0.23 ± 0.01	—	1.22 ± 0.07	—
Air-sea exchange (a-s)	0.20 ± 0.13	28.51 ± 16.16	1.01 ± 0.70	38.97 ± 23.50
Mixing (mix)	−0.04 ± 0.01	−6.42 ± 2.02	−0.20 ± 0.05	−8.20 ± 2.67
Biological production/respiration (bio)	0.11 ± 0.14	17.22 ± 18.69	0.57 ± 0.65	24.10 ± 24.97
$CaCO_3$ formation/dissolution (cal)	−0.08 ± 0.05	−11.02 ± 5.73	−0.34 ± 0.20	−13.41 ± 6.94
Nonlinear term (non)	0.03 ± 0.04	3.90 ± 3.89	0.02 ± 0.08	1.26 ± 2.40

Note. Relative importance is also shown (%ΔpH and %ΔΩ). Note that the second temperature effect associated with CO_2 solubility is not considered when the relative importance is calculated, and except for this term, all other results are based on the 1-D model described in section 2.4. Positive values denote increases of pH and Ω_{arag} and negative values decreases of pH and Ω_{arag}. [a]Here the temperature effect only refers to the first temperature effect associated with thermodynamically driven acid-base equilibrium of the CO_2 system and does not include the second temperature effect associated with temperature-driven CO_2 solubility, which is included in the air-sea exchange term.

and Table 3). That is, the second temperature effect dominates the net temperature effect and would play a very important role in the seasonal variability of $pH_{@in\ situ}$ and $\Omega_{arag@in\ situ}$. Also, it suggests that the net temperature effect would have a minor influence on pH but a substantial influence on Ω_{arag}, and the contrast between the first temperature effects on pH and Ω_{arag} to some extent decreases the seasonal amplitude of pH but increases the seasonal amplitude of Ω_{arag} (Table 3). This implies that the maximum or minimum of pH and Ω_{arag} in seasonal cycles would be often out of sync (e.g., Omar et al., 2016; Takahashi et al., 2014; Xue et al., 2017).

In addition, we find that the contrast between the first temperature effects on pH and Ω_{arag} is the biggest difference among their controlling processes. The property-property plots of $pH_{@25}$ with SST, SSS, and AOU are very similar to the property-property plots of $\Omega_{arag@25}$ with SST, SSS, and AOU (Figure 5). The model results (Figures 6 and 7) also show that except for the first temperature effect, the controlling processes of pH and Ω_{arag} are almost the same. Realizing the opposite influence on pH and Ω_{arag} by the first temperature effect is important for understanding the controls and dynamics of pH and Ω_{arag} on different time scales. For instance, the opposite influence on pH and Ω_{arag} by the first temperature effect leads to latitudinal differences (spatial variability) between pH and Ω_{arag} in open oceans (Jiang et al., 2019). However, this influence on the spatial distributions of $pH_{@in\ situ}$ and $\Omega_{arag@in\ situ}$ is not obvious in the JZB during the two cruises (Figures 4e–4h) due to the relatively homogeneous spatial distributions of SST as shown in Figures 3a and 3b.

3.3.2. The Second Temperature Effect and Air-Sea Exchange

In practice, the interaction between the first and the second temperature effects usually behaves as the interaction between the first temperature effect and air-sea CO_2 exchange, since the second temperature effect is realized mainly via air-sea CO_2 exchange. The 1-D model results show that on average, from spring to summer, air-sea CO_2 exchange would increase pH and Ω_{arag} by 0.20 ± 0.13 and 1.01 ± 0.70, respectively (Table 3). The contribution by air-sea CO_2 exchange is generally consistent with the pH (0.23 ± 0.01) and Ω_{arag} variability (1.22 ± 0.07) by the second temperature effect (Table 3), suggesting that the second temperature effect is realized mainly via air-sea CO_2 exchange. As discussed in section 3.3.1, the influence on pH from air-sea exchange (29%) is almost completely offset by that from the first temperature effect (−28%, Table 3), resulting in a relatively small seasonal variability of pH from spring to summer in the JZB. In contrast, the influences on Ω_{arag} from the first temperature effect (9%) and air-sea exchange (39%, Table 3) reinforce each other, leading to a relatively large seasonal variability of Ω_{arag}. That is, the second temperature effect or air-sea exchange plays an important role in the seasonal variability of pH and Ω_{arag}. Given the possible influence of other processes on air-sea CO_2 exchange such as biological processes and the uncertainty in quantifying the second temperature effect mainly due to air-sea CO_2 disequilibrium in the ocean, hereafter, the second temperature effect is included in the air-sea exchange term, and instead temperature effect only refer to the first temperature effect especially in the 1-D model, if not otherwise specified.

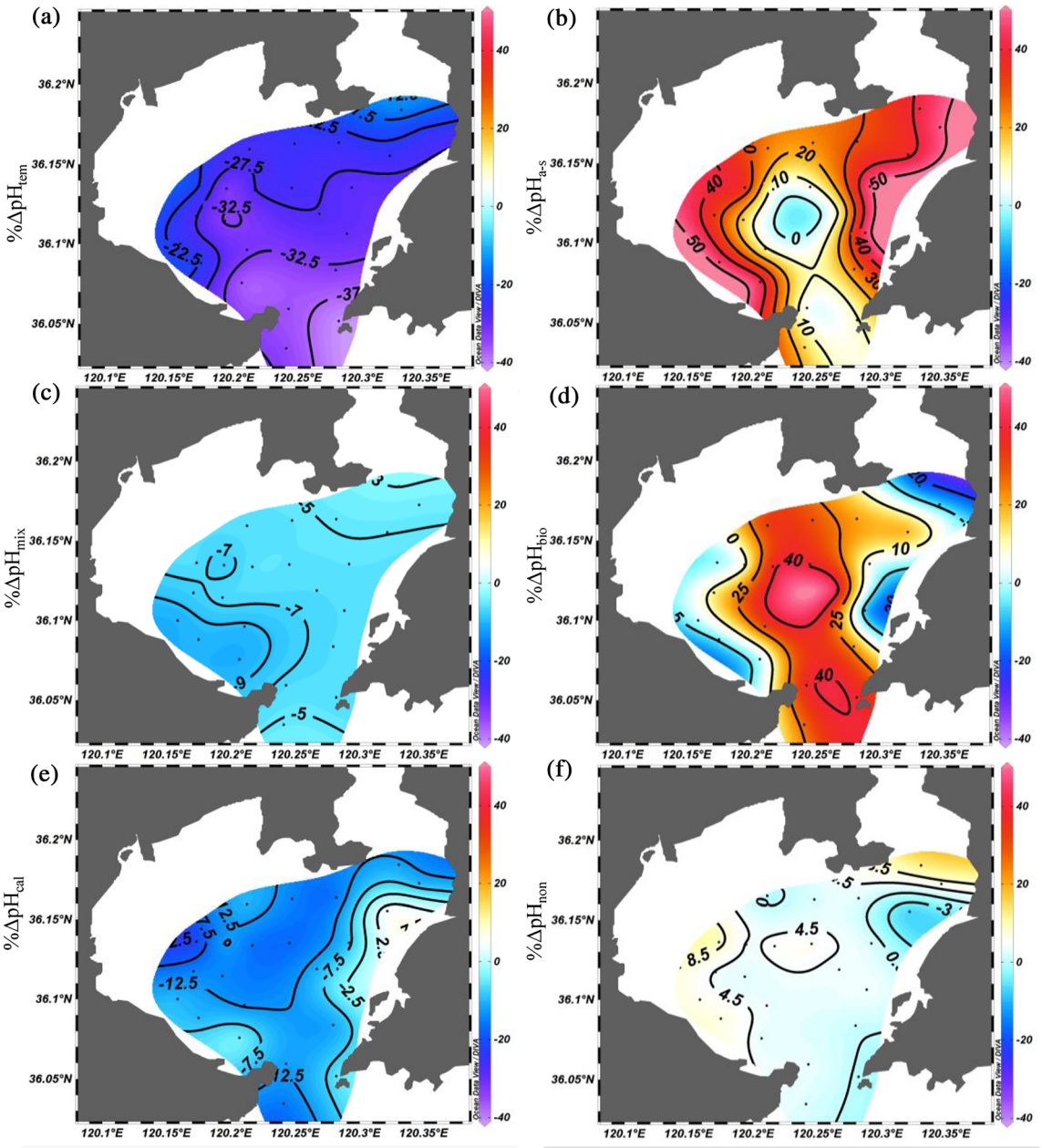

Figure 6. Relative importance of (a) temperature variability ($\%\Delta pH_{tem}$), (b) air-sea exchange ($\%\Delta pH_{a-s}$), (c) mixing ($\%\Delta pH_{mix}$), (d) biological production/respiration ($\%\Delta pH_{bio}$), and (e) calcium carbonate formation/dissolution ($\%\Delta pH_{cal}$) to pH variability from spring to summer as well as (f) the nonlinear term ($\%\Delta pH_{non}$). Results are based on the 1-D model described in section 2.4. Positive values denote pH increases and negative values pH decreases.

3.4. Influences of Mixing and Biological Activities on Seasonal Variability of pH and Ω_{arag}

Here, we examine the influences from mixing between terrestrial inputs and ocean and biological processes on the seasonal variability of pH and Ω_{arag} through both the qualitative analyses and the 1-D model. We find that the mixing effect on the seasonal variability of pH and Ω_{arag} is minor. This is because usually terrestrial inputs would decrease both salinity and pH of coastal oceans such as in the JZB (Table 1) (Li et al., 2017; Xue & Cai, 2020). As a result, if mixing exerted a large influence on the seasonal variability of pH and Ω_{arag}, pH and Ω_{arag} would decrease with decreasing SSS as shown by the theoretical mixing lines (Figures 5e and 5f). However, we observe in the JZB from April to August both pH and Ω_{arag} increase with decreasing SSS. Thus, we infer that the mixing effect on the seasonal variability of pH and Ω_{arag} may be minor. This result is well

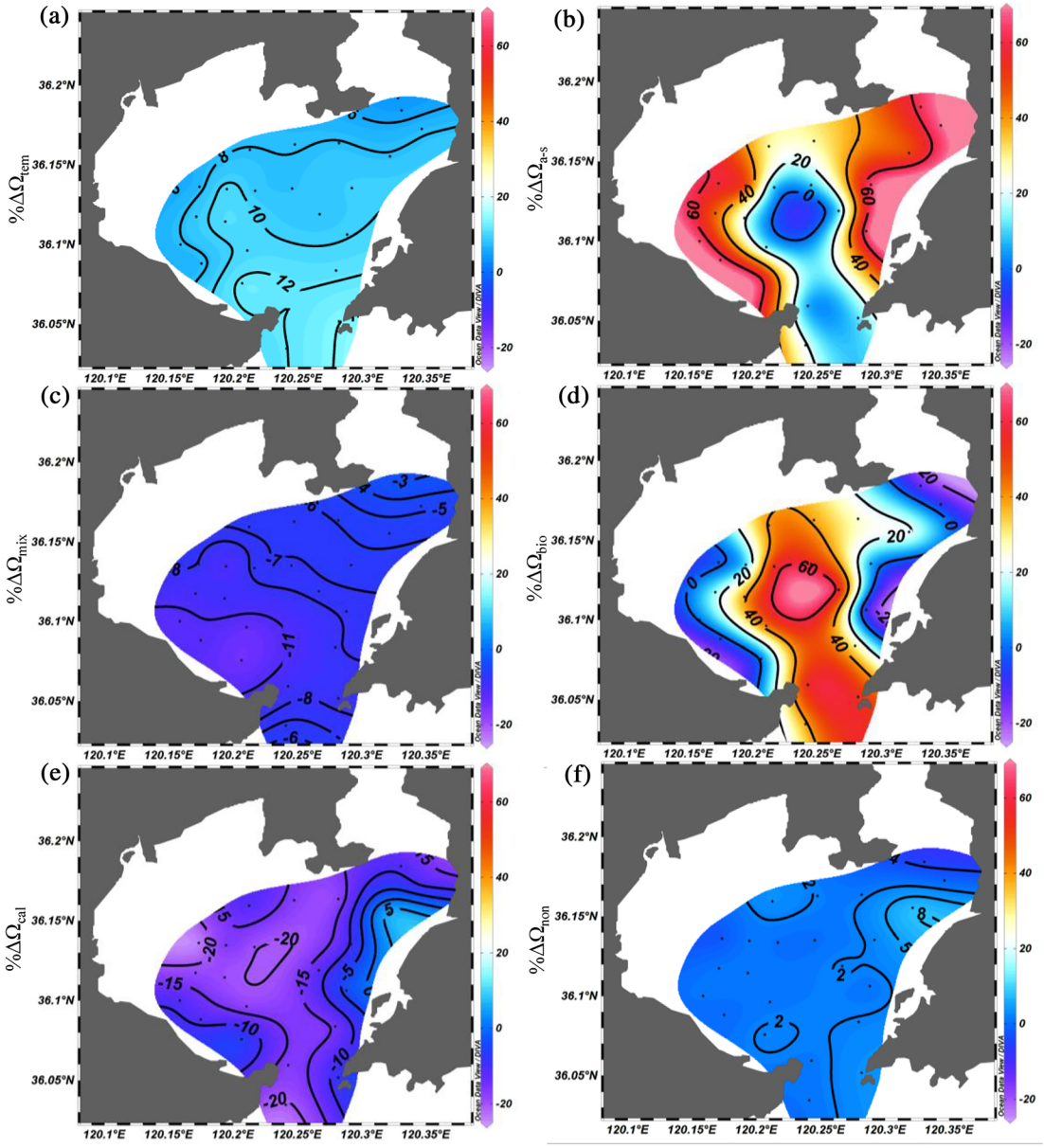

Figure 7. Relative importance of (a) temperature variability ($\%\Delta\Omega_{tem}$), (b) air-sea exchange ($\%\Delta\Omega_{a-s}$), (c) mixing ($\%\Delta\Omega_{mix}$), (d) biological production/respiration ($\%\Delta\Omega_{bio}$), and (e) calcium carbonate formation/dissolution ($\%\Delta\Omega_{cal}$) to Ω_{arag} variability from spring to summer as well as (f) the nonlinear term ($\%\Delta\Omega_{non}$). Results are based on the 1-D model described in section 2.4. Positive values denote Ω_{arag} increases and negative values Ω_{arag} decreases.

consistent with the model result, which shows that mixing between terrestrial inputs and ocean just plays a minor role in the seasonal variability of pH and Ω_{arag}. On average, mixing would decrease pH and Ω_{arag} by 0.04 and 0.20 from spring to summer, just accounting for −6% and −8% of the total seasonal variability, respectively (Table 3).

Note that the composite terrestrial end-member values will vary mainly due to spatial differences in end-member values of estuaries around the JZB, which may cause uncertainties for the 1-D mode. To examine the possible influence from variability of terrestrial end-member values, we use the average plus standard deviation and average minus standard deviation as the upper and lower bounds of terrestrial end-member values, respectively. We find when the upper and lower bounds of terrestrial end-member values are considered, mixing would decrease pH and Ω_{arag} by 0.04 ± 0.03 and 0.20 ± 0.14 from spring to summer, respectively (Figures 5e and 5f). It indicates though the contribution from mixing is sensitive to

the variability of the composite terrestrial end-member values, it does not influence our conclusion (Table 3). The good agreement between the results from the qualitative analyses and from the 1-D model suggests that the 1-D model is robust in quantifying the mixing effect. Also, it means that biological effect would be well quantified by the 1-D model, considering that the biggest uncertainty of the 1-D model may originate from the mixing term, which directly affects the estimation of biological effect.

Biological production will consume CO_2 and produce oxygen, thus increasing pH and Ω_{arag} and decreasing AOU. Therefore, if biological production/respiration exerted a large influence on the seasonal variability of pH and Ω_{arag}, pH and Ω_{arag} would increase with decreasing AOU as shown by the Redfield lines (Figures 5g and 5h). From April to August in the JZB, we observe both pH and Ω_{arag} increase with decreasing AOU, but they do not well follow the Redfield lines. Thus, we infer that biological production from spring to summer may play an important but not a dominant role in the seasonal variability of pH and Ω_{arag}. This result is in good agreement with the model result, which shows that biological production plays an important role in the seasonal variability of pH and Ω_{arag}. From spring to summer, on average, biological production would increase pH and Ω_{arag} by 0.11 and 0.57, accounting for 17% and 24% of the total seasonal variability, respectively (Table 3). Also, model results show that on average, $CaCO_3$ formation would decrease pH and Ω_{arag} by 0.08 and 0.34, accounting for −11% and −13% of the total seasonal variability, respectively (Table 3). However, compared to biological production, the contribution from $CaCO_3$ formation is small. The pH and Ω_{arag} decrease induced by $CaCO_3$ formation can be completely offset by the biological production induced pH and Ω_{arag} increase, and thus on the whole, biological processes increase pH and Ω_{arag} from spring to summer in the JZB (Table 3). Overall, both the qualitative analyses and the 1-D model indicate that for the entire study area, air-sea exchange followed by biological production plays the most important role in the seasonal variability of pH and Ω_{arag} from spring to summer (Table 3).

3.5. Spatial Difference of Processes Controlling Seasonal Variability of pH and Ω_{arag}

Here we show the spatial difference of controlling processes based on the 1-D model. Considering the spatial patterns of relative importance and absolute contribution of each process discussed in the 1-D model (Figures 6 and 7 and Figures S2 and S3) are very similar, we just show the spatial patterns of relative importance in the main text. We find that the contribution of each process to the seasonal variability of pH and Ω_{arag} shows a large spatial heterogeneity (Figures 6 and 7). In the entire study area, increased temperature from spring to summer decreases pH (Figure 6a). ΔpH_{tem} ranges from −0.20 to −0.15 (Figure S2) and $\%\Delta pH_{tem}$ varies from −37% to −12.5%, with strong temperature influences in the southern part of the study area (Figure 6a) where there is a rapid warming from spring to summer (Figures 3a and 3b). In contrast, from spring to summer in the whole study area, air-sea exchange increases pH. It plays a dominant role in the seasonal variability of pH in shallow nearshore areas with water depths of less than ~10 m, with $\%\Delta pH_{a\text{-}s}$ of >40% (Figure 6b), whereas its influence is minor in the central part of the JZB due to deep water depths of greater than ~10 m (Figure 2). Different from air-sea exchange, in the central part of the JZB, biological production plays a dominant role in the seasonal variability of pH with $\%\Delta pH_{bio}$ of >25%, while in nearshore areas, biological respiration/degradation slightly decreases pH (Figure 6d). This model result is consistent with the incubation experiment result that the excess CO_2 especially along the eastern coast of the JZB is mainly from the aerobic respiration (Han et al., 2017).

Compared to influences from temperature, air-sea exchange, and biological production/respiration, influences from mixing between terrestrial inputs and ocean and $CaCO_3$ formation/dissolution are relatively small. ΔpH_{mix} ranges from −0.07 to −0.03 (Figure S2), and $\%\Delta pH_{mix}$ varies from −9% to −3%, with relatively strong influences in the west and northwest of the study area (Figure 6c) possibly due to strong river inputs in summer (Figures 3c and 3d). $CaCO_3$ formation decreases pH in most part of the JZB especially in the north and the northwest with $\%\Delta pH_{cal}$ between −12.5% and −7.5%, and just in a small portion of the eastern part, $CaCO_3$ dissolution increases pH with $\%\Delta pH_{cal}$ of ~2.5% (Figure 6e). This result is in good agreement with that based on an isotopic method (Yang et al., 2018), which again indicates the robustness of the 1-D model. Compared to the controlling processes considered in this work, the nonlinear effect of pH is relatively minor with $\%\Delta pH_{non} < 9\%$ (Figure 6f).

Different from pH, in the entire study area, increased temperature from spring to summer increases Ω_{arag} (Figure 7a). $\Delta\Omega_{tem}$ ranges from 0.18 to 0.24 (Figure S3), and $\%\Delta\Omega_{tem}$ varies from 6% to 12%, with strong

temperature influences in the southern part of the study area (Figure 7a) due to a rapid warming from spring to summer (Figures 3a and 3b). Further, we find, except for the temperature effect or the first temperature effect, that processes controlling pH and Ω_{arag} are very similar (Figures 6 and 7). For example, in nearshore areas, air-sea exchange plays a dominant role in the seasonal variability of Ω_{arag} with $\%\Delta\Omega_{a\text{-}s}$ of >40%, whereas biological production plays a dominant role in the central part with $\%\Delta\Omega_{bio}$ of over 40% (Figure 7). Overall, from spring to summer, increased temperature decreases pH but increases Ω_{arag} in the entire study area; air-sea exchange plays a dominant role in the nearshore area, while biological production plays a dominant role in the central part.

4. Conclusions

Realizing the opposite influence on pH and Ω_{arag} by the first temperature effect is important for understanding the controls and dynamics of pH and Ω_{arag} on different time scales. The contrast between the first temperature effects on pH and Ω_{arag} is the biggest difference among their controlling processes. It makes the net temperature effect have a minor influence on pH but a large influence on Ω_{arag}, and to some extent decreases the seasonal amplitude of pH but increases the seasonal amplitude of Ω_{arag} such as in the JZB. Also, it causes differences in spatial distributions of pH and Ω_{arag} (e.g., latitudinal difference) (Jiang et al., 2019) and even the unsynchronization of the maximum or minimum of pH and Ω_{arag} in seasonal cycles (e.g., Omar et al., 2016; Takahashi et al., 2014; Xue et al., 2017).

Both the qualitative analyses and the 1-D model indicate that in the JZB, from spring to summer, air-sea exchange or the second temperature effect dominates the seasonal variability of pH and Ω_{arag} in shallow nearshore areas, while biological production plays the most important role in the central part of the JZB. This work would improve the understanding of the natural variability of acidification parameters and their controlling mechanisms.

Conflict of Interest

All authors have no conflict of interest.

Data Availability Statement

The data set used in this study has been archived by the NOAA National Centers for Environmental Information (NCEI) with assigned Accession Number 0208682. The link to the metadata page is https://www.nodc.noaa.gov/ocads/data/0208682.xml.

Acknowledgments
This work was supported by the Basic Scientific Fund for National Public Research Institutes of China (2016Q01, 2019S05) and the Open Fund of Laboratory for Marine Ecology and Environmental Science, Qingdao National Laboratory for Marine Science and Technology (LMEES201808). We thank Chen Kan, Xu Hanyue, and Wu Linni for sampling collection.

References

Albright, R., Takeshita, Y., Koweek, D. A., Ninokawa, A., Wolfe, K., Rivlin, T., et al. (2018). Carbon dioxide addition to coral reef waters suppresses net community calcification. *Nature*, *555*(7697), 516–519. https://doi.org/10.1038/nature25968

Benson, B. B., & Krause, D. Jr. (1984). The concentration and isotopic fractionation of oxygen dissolved in freshwater and seawater in equilibrium with the atmosphere. *Limnology and Oceanography*, *29*(3), 620–632. https://doi.org/10.4319/lo.1984.29.3.0620

Cai, W.-J., Hu, X., Huang, W., Murrell, M. C., Lehrter, J. C., Lohrenz, S. E., et al. (2011). Acidification of subsurface coastal waters enhanced by eutrophication. *Nature Geoscience*, *4*(11), 766–770. https://doi.org/10.1038/ngeo1297

Cai, W.-J., Wang, Y., & Hodson, R. E. (1998). Acid-base properties of dissolved organic matter in the estuarine waters of Georgia, USA. *Geochimica et Cosmochimica Acta*, *62*(3), 473–483. https://doi.org/10.1016/S0016-7037(97)00363-3

Caldeira, K., & Wickett, M. E. (2003). Oceanography: Anthropogenic carbon and ocean pH. *Nature*, *425*(6956), 365. https://doi.org/10.1038/425365a

Chen, C., Ji, R., Zheng, L., Zhu, M., & Rawson, M. (1999). Influences of physical processes on the ecosystem in Jiaozhou Bay: A coupled physical and biological model experiment. *Journal of Geophysical Research*, *104*(C12), 29925–29949. https://doi.org/10.1029/1999JC900203

Chen, C.-T. A. (1978). Decomposition of calcium carbonate and organic carbon in the deep oceans. *Science*, *201*(4357), 735–736. https://doi.org/10.1126/science.201.4357.735

Cooley, S. R., Mathis, J. T., Yates, K. K., & Turley, C. (2012). Frequently asked questions about ocean acidification. U.S. Ocean Carbon and Biogeochemistry Program and the UK Ocean Acidification Research Program, Version 2. 24 September 2012. www.whoi.edu/OCB-OA/FAQs

Deng, X., Hu, Y., Liu, C., Yang, G., Lu, X., & Zhang, H. (2016). Distributions and sessonal variations of carbonate system in the Jiaozhou Bay, China. *Oceanologia et Limnologia Sinica*, *47*(1), 234–244. (in Chinese with English abstract)

Dickson, A. G., & Millero, F. J. (1987). A comparison of the equilibrium constants for the dissociation of carbonic acid in seawater media. *Deep Sea Research Part A. Oceanographic Research Papers*, *34*(10), 1733–1743.

Doney, S. C., Fabry, V. J., Feely, R. A., & Kleypas, J. A. (2009). Ocean acidification: The other CO_2 problem. *Annual Review of Marine Science*, *1*(1), 169–192. https://doi.org/10.1146/annurev.marine.010908.163834

Dong, X., Huang, H., Zheng, N., Pan, A., Wang, S., Huo, C., et al. (2017). Acidification mediated by a river plume and coastal upwelling on a fringing reef at the east coast of Hainan Island, northern South China Sea. *Journal of Geophysical Research: Oceans*, *122*, 7521–7536. https://doi.org/10.1002/2017JC013228

Fassbender, A. J., Sabine, C. L., & Feifel, K. M. (2016). Consideration of coastal carbonate chemistry in understanding biological calcification. *Geophysical Research Letters*, *43*, 4467–4476. https://doi.org/10.1002/2016GL068860

Feely, R. A., Sabine, C. L., Hernandez-Ayon, J. M., Ianson, D., & Hales, B. (2008). Evidence for upwelling of corrosive "acidified" water onto the continental shelf. *Science*, *320*(5882), 1490–1492. https://doi.org/10.1126/science.1155676

Friedlingstein, P., Jones, M. W., O'Sullivan, M., Andrew, R. M., Hauck, J., Peters, G. P., et al. (2019). Global carbon budget 2019. *Earth System Science Data*, *11*(4), 1783–1838. https://doi.org/10.5194/essd-11-1783-2019

Fu, M., Wang, Z., Li, Y., Li, R., Lu, R., Sun, P., & Xia, B. (2009). Study on size-fraction and carbon fixation of phytoplankton primary productivity in Jiaozhou Bay. *Advances in Marine Science*, *27*, 357–366. (in Chinese with English abstract)

Gao, Z., Yang, D., Qin, J., Xiang, L., & Zhang, K. (2008). The land-sourced pollution in the Jiaozhou Bay. *Chinese Journal of Oceanology and Limnology*, *26*(2), 229–232. https://doi.org/10.1007/s00343-008-0229-7

Gruber, N., Clement, D., Carter, B. R., Feely, R. A., van Heuven, S., Hoppema, M., et al. (2019). The oceanic sink for anthropogenic CO_2 from 1994 to 2007. *Science*, *363*(6432), 1193–1199. https://doi.org/10.1126/science.aau5153

Hagens, M., & Middelburg, J. J. (2016). Attributing seasonal pH variability in surface ocean waters to governing factors. *Geophysical Research Letters*, *43*, 12,528–12,537. https://doi.org/10.1002/2016gl071719

Han, P., Li, Y., Yang, X., Xue, L., & Zhang, L. (2017). Effects of aerobic respiration and nitrification on dissolved inorganic nitrogen and carbon dioxide in human-perturbed eastern Jiaozhou Bay, China. *Marine Pollution Bulletin*, *124*(1), 449–458. https://doi.org/10.1016/j.marpolbul.2017.07.055

Jiang, L.-Q., Carter, B. R., Feely, R. A., Lauvset, S. K., & Olsen, A. (2019). Surface ocean pH and buffer capacity: Past, present and future. *Scientific Reports*, *9*(1), 18624. https://doi.org/10.1038/s41598-019-55039-4

Lewis, E., Wallace, D., & Allison, L. J. (1998). Program developed for CO_2 systems calculations, ORNL/CDIAC 105, Carbon Dioxide Information Analysis Center. Oak Ridge, TN: Oak Ridge National Laboratory US Department of Energy. https://doi.org/10.2172/639712

Li, K., Li, J., Li, Y., He, J., Guo, Q., Liang, S., & Wang, X. (2018). Linking water quality with the total pollutant load control management for nitrogen in Jiaozhou Bay, China. *Ecological Indicators*, *85*, 57–66. https://doi.org/10.1016/j.ecolind.2017.10.019

Li, X., Song, J., Niu, L., Yuan, H., Li, N., & Gao, X. (2007). Role of the Jiaozhou Bay as a source/sink of CO_2 over a seasonal cycle. *Scientia Marina*, *71*(3), 441–450.

Li, Y., Yang, X., Han, P., Xue, L., & Zhang, L. (2017). Controlling mechanisms of surface partial pressure of CO_2 in Jiaozhou Bay during summer and the influence of heavy rain. *Journal of Marine Systems*, *173*, 49–59. https://doi.org/10.1016/j.jmarsys.2017.04.006

Mehrbach, C., Culberson, C. H., Hawley, J. E., & Pytkowicz, R. M. (1973). Measurement of the apparent dissociation constants of carbonic acid in seawater at atmospheric pressure. *Limnology and Oceanography*, *18*(6), 897–907. https://doi.org/10.4319/lo.1973.18.6.0897

Morse, J. W., Arvidson, R. S., & Lüttge, A. (2007). Calcium carbonate formation and dissolution. *Chemical Reviews*, *107*(2), 342–381. https://doi.org/10.1021/cr050358j

Mucci, A. (1983). The solubility of calcite and aragonite in seawater at various salinities, temperatures, and one atmosphere total pressure. *American Journal of Science*, *283*(7), 780–799. https://doi.org/10.2475/ajs.283.7.780

Omar, A. M., Skjelvan, I., Erga, S. R., & Olsen, A. (2016). Aragonite saturation states and pH in western Norwegian fjords: seasonal cycles and controlling factors, 2005–2009. *Ocean Science*, *12*, 937–951. https://doi.org/10.5194/os-12-937-2016

Redfield, A. C., Ketchum, B. H., & Richards, F. A. (1963). The influence of organisms on the composition of sea water. In M. N. Hill (Ed.), *The composition of seawater: Comparative and descriptive oceanography*, *The sea: Ideas and observations on progress in the study of the seas* (Vol. 2, pp. 26–77). New York: Interscience Publishers.

Sarmiento, J. L., & Gruber, N. (2006). *Ocean biogeochemical dynamics* (1st ed., pp. 1–503). Princeton, NJ: Princeton University Press. https://doi.org/10.1515/9781400849079

Sutton, A. J., Sabine, C. L., Feely, R. A., Cai, W. J., Cronin, M. F., McPhaden, M. J., et al. (2016). Using present-day observations to detect when anthropogenic change forces surface ocean carbonate chemistry outside preindustrial bounds. *Biogeosciences*, *13*(17), 5065–5083. https://doi.org/10.5194/bg-13-5065-2016

Sweeney, C., Gloor, E., Jacobson, A. R., Key, R. M., McKinley, G., Sarmiento, J. L., & Wanninkhof, R. (2007). Constraining global air-sea gas exchange for CO_2 with recent bomb ^{14}C measurements. *Global Biogeochemical Cycles*, *21*, GB2015. https://doi.org/10.1029/2006GB002784

Takahashi, T., Sutherland, S. C., Chipman, D. W., Goddard, J. G., & Ho, C. (2014). Climatological distributions of pH, pCO_2, total CO_2, alkalinity, and $CaCO_3$ saturation in the global surface ocean, and temporal changes at selected locations. *Marine Chemistry*, *164*, 95–125. https://doi.org/10.1016/j.marchem.2014.06.004

Waldbusser, G. G., Gray, M. W., Hales, B., Langdon, C. J., Haley, B. A., Gimenez, I., et al. (2016). Slow shell building, a possible trait for resistance to the effects of acute ocean acidification. *Limnology and Oceanography*, *61*(6), 1969–1983. https://doi.org/10.1002/lno.10348

Wei, Q., Wang, B., Yao, Q., Xue, L., Sun, J., Xin, M., & Yu, Z. (2019). Spatiotemporal variations in the summer hypoxia in the Bohai Sea (China) and controlling mechanisms. *Marine Pollution Bulletin*, *138*, 125–134. https://doi.org/10.1016/j.marpolbul.2018.11.041

Weiss, R. F. (1974). Carbon dioxide in water and seawater: The solubility of a non-ideal gas. *Marine Chemistry*, *2*(3), 203–215. https://doi.org/10.1016/0304-4203(74)90015-2

Xu, Y. Y., Cai, W.-J., Gao, Y., Wanninkhof, R., Salisbury, J., Chen, B., et al. (2017). Short-term variability of aragonite saturation state in the central Mid-Atlantic Bight. *Journal of Geophysical Research: Oceans*, *122*, 4274–4290. https://doi.org/10.1002/2017JC012901

Xue, L., & Cai, W.-J. (2020). Total alkalinity minus dissolved inorganic carbon as a proxy for deciphering ocean acidification mechanisms. *Marine Chemistry*, *222*, 103791. https://doi.org/10.1016/j.marchem.2020.103791

Xue, L., Cai, W.-J., Hu, X., Sabine, C., Jones, S., Sutton, A. J., et al. (2016b). Sea surface carbon dioxide at the Georgia time series site (2006–2007): Air-sea flux and controlling processes. *Progress in Oceanography*, *140*, 14–26. https://doi.org/10.1016/j.pocean.2015.09.008

Xue, L., Cai, W.-J., Sutton, A. J., & Sabine, C. (2017). Sea surface aragonite saturation state variations and control mechanisms at the Gray's Reef time-series site off Georgia, USA (2006–2007). *Marine Chemistry*, *195*, 27–40. https://doi.org/10.1016/j.marchem.2017.05.009

Xue, L., Cai, W.-J., Takahashi, T., Gao, L., Wanninkhof, R., Wei, M., et al. (2018). Climatic modulation of surface acidification rates through summertime wind forcing in the Southern Ocean. *Nature Communications*, *9*(1), 3240. https://doi.org/10.1038/s41467-018-05443-7

Xue, L., Wang, H., Jiang, L., Cai, W.-J., Wei, Q., Song, H., et al. (2016a). Aragonite saturation state in a monsoonal upwelling system off Java, Indonesia. *Journal of Marine Systems*, *153*, 10–17. https://doi.org/10.1016/j.jmarsys.2015.08.003

Yang, W., Gao, H., Liu, H., Gao, Y., & Fu, M. (2007). Preliminary study on effects of scallop cultivation on water quality in Jiaozhou Bay. *Transactions of Oceanology and Limnology*, *2*, 86–93. (in Chinese with English abstract)

Yang, X., Xue, L., Li, Y., Han, P., Liu, X., Zhang, L., & Cai, W. J. (2018). Treated wastewater changes the export of dissolved inorganic carbon and its isotopic composition and leads to acidification in coastal oceans. *Environmental Science & Technology*, *52*(10), 5590–5599. https://doi.org/10.1021/acs.est.8b00273

Zhang, J. (2007). Watersheds nutrient loss and eutrophication of the marine recipients: A case study of the Jiaozhou Bay, China. *Water, Air, & Soil Pollution: Focus*, *7*(6), 583–592. https://doi.org/10.1007/s11267-007-9130-1

Zhang, L., Chen, G., & Ji, R. (1992). The calcium and magnesium in seawaters of the Jiaozhou Bay. *Oceanologia et Limnologia Sinica*, *23*(5), 498–504. (in Chinese with English abstract)

Zhao, Y., Liu, J., Uthaipan, K., Song, X., Xu, Y., He, B., et al. (2020). Dynamics of inorganic carbon and pH in a large subtropical continental shelf system: Interaction between eutrophication, hypoxia, and ocean acidification. *Limnology and Oceanography*, lno.11393. https://doi.org/10.1002/lno.11393